# Thermal stability, crystallization kinetics, and grain growth in an amorphous Al$_{85}$Ce$_5$Ni$_8$Co$_2$ alloy

Á. Révész

*Department of Physics, Faculty of Sciences, Universitat Autònoma Barcelona, Edifici Cc,*
*08193 Bellaterra, Barcelona, Spain, and Department of General Physics, Eötvös University,*
*H-1518 Budapest, P.O.B. 32, Hungary*

L.K. Varga

*Research Institute for Solid State Physics and Optics, Hungarian Academy of Sciences,*
*H-1525 Budapest, P.O.B. 49, Hungary*

S. Suriñach and M.D. Baró

*Department of Physics, Faculty of Sciences, Universitat Autònoma Barcelona, Edifici Cc,*
*08193 Bellaterra, Barcelona, Spain*

Thermal stability and crystallization kinetics of the melt-quenched amorphous Al$_{85}$Ce$_5$Ni$_8$Co$_2$ alloy were investigated by x-ray diffraction and differential scanning calorimetry (DSC). The glass transition was followed by a supercooled liquid region (21 °C) and then by a two-step crystallization process. The final microstructure contained Al$_3$Ce, α–Al, Al$_3$Ni, and Al$_9$Co$_2$ phases. Isothermal annealing of the as-quenched samples in the range of 275–285 °C showed that both crystallization reactions occurred through a nucleation and growth process. Continuous heating DSC measurements following pre-anneals for different times were also carried out to study the crystallization kinetics and the stability of the material. The Avrami analysis of the isothermal DSC-curves revealed that the 3-dimensional nucleation and growth process became more dominant with increasing annealing temperature. The average specific grain boundary energy corresponded to high-angle grain boundaries and indicated independent nucleation events.

## I. INTRODUCTION

Conventional aluminum alloys have been well known for their use as light-weight components in engineering applications, particularly in the aerospace industry, for some time. Recently, it has been found that rapidly quenched Al-based alloys[1,2] exhibit better mechanical properties, with high tensile strength and good ductility.[3] The crystallization behavior of the Al–Ni–Y ternary[4,5] and Al–Ni–Y–Co[6–9] quaternary systems indicates a three-stage process with primary crystallization of the α–Al phase. Primary crystallization in the residual amorphous matrix is an important method for a well-controlled production of nanophase composite materials.[10,11] The crystallization sequence in the Al–Ni–Ce system, however, strongly depends on the concentration of the constituents. As was shown by Tsai *et al.,*[12] the single precipitation α–Al is not observed above 4 at.% Ce.

This paper is concerned with the thermal stability, crystallization sequence, and the isothermal and nonisothermal crystallization kinetics in the Al$_{85}$Ce$_5$Ni$_8$Co$_2$ alloy.[13,14] The effect of Co addition on the thermal stability of Al$_{85}$Ni$_{10}$Ce$_5$ was also studied.

## II. EXPERIMENTAL

### A. Sample preparation

Ingots were prepared by induction-melting a mixture of pure (99.99 wt%) Al, Ce, Ni, and Co elements. The Al$_{85}$Ce$_5$Ni$_8$Co$_2$ ribbon (3–4 mm wide and about 20 μm thick) was obtained using a single roller melt spinning technique in inert atmosphere with a Cu wheel rotating at a peripheral velocity of 39 m/s. The ribbon was ductile and in the form of several 10-cm-long pieces.

### B. Differential scanning calorimetry measurements

A Perkin Elmer DSC-7 differential scanning calorimeter (Shelton, CT) was used to carry out continuous heating experiments and isothermal annealings to investigate the thermal stability and crystallization kinetics. To protect the samples against oxidation, all measurements were done in an argon flux. The temperature and the enthalpy were calibrated with pure In and Al. The calibration procedure of the apparatus ensures temperature measurements with less than 0.05% error and enthalpy output measurements with a 2% error.

Continuous heating experiments up to 550 °C were performed at scan rates in the range of 2.5–80 K min$^{-1}$, followed by a second scan to obtain the calorimetric baseline. From the shift of the differential scanning calorimetry (DSC) peaks with increasing heating rate, the apparent activation energy of the crystallization process was determined using the Kissinger analysis.[15] Isothermal heat treatments were carried out by heating the samples of the heat-treatment temperature at 100 K min$^{-1}$.

## C. X-ray diffraction

The amorphous nature of the as-quenched ribbon and the crystallization phases were examined by x-ray diffraction (XRD) using Cu K$_\alpha$ radiation on a Philips X'pert powder diffractometer (Almelo, The Netherlands) in θ-2θ geometry. The average crystalline sizes of the heat-treated samples were quantified from the XRD patterns by a fitting program.[16]

## III. RESULTS

### A. Thermal stability

Continuous heating DSC curves obtained at different heating rates are shown in Fig. 1. These curves present a glass transition ($T_g$), followed by a supercooled liquid region ($\Delta T_x$) and two exothermic crystallization peaks ($T_{x1}$, $T_{x2}$). The temperatures of the main transformations are presented in Table I. At the heating rate of 20 K min$^{-1}$ the onset of the crystallization process of the Al$_{85}$Ni$_8$Ce$_5$Co$_2$ alloy occurs at about 40 °C higher than the Al$_{85}$Ni$_{10}$Ce$_5$ alloy,[13,14] indicating that the Co substitution of Ni results in an increased thermal stability. The transformation enthalpies were obtained as

the area of the first and second exothermic peak and the estimated values of $\Delta H_1$ and $\Delta H_2$ were 75 ± 5 and 40 ± 3 J/g, respectively.

Also shown in Fig. 1 as an inset are the Kissinger plots, from which the apparent activation energy values were at 3.9 ± 0.5 and 2.0 ± 0.3 eV for the first and second crystallization process, respectively. The considerably higher apparent activation energy for the first crystallization also refers to a thermally stable state and suggests that the crystallization takes place through a nucleation and growth process.[10,17] These values are similar to those obtained for the Al$_{85}$Y$_5$Ni$_8$Co$_2$[9] and Al$_{84}$Y$_9$Ni$_5$Co$_2$[6] alloys.

Isothermal annealing of the as-quenched amorphous alloy was carried out for $t_{ann}$ = 120 min at several temperatures ($T_{ann}$) in the range of 275–285 °C in order to study the crystallization mechanisms. As can be seen in Fig. 2, each isotherm starts with an incubation period ($t_0$) and is followed by two exothermic peaks corresponding to the two crystallization processes obtained during continuous heating, as was confirmed by the lack of any thermal effects in the continuous heating carried out after

TABLE I. Transformation parameters obtained from the continuous heating experiments for the Al$_{85}$Ce$_5$Ni$_8$Co$_2$ alloy. See text for notation.

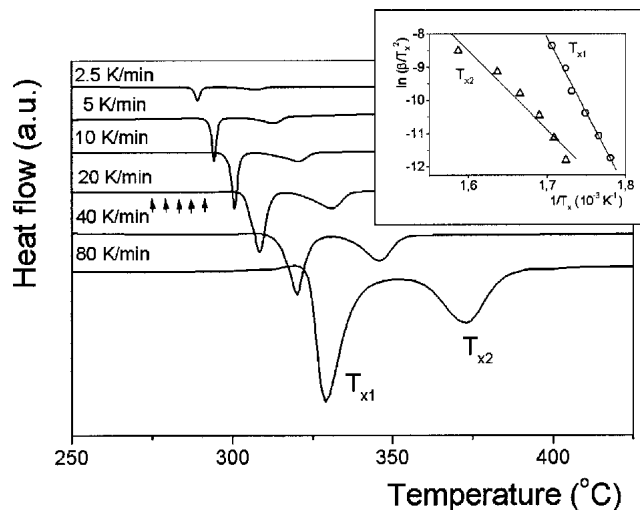| β (K/min) | $T_g$ (°C) | $T_{x1}$ (°C) | $\Delta T_x$ (°C) | $T_{x2}$ (°C) |
|---|---|---|---|---|
| 2.5 | ⋯ | 289.0 | ⋯ | 307.5 |
| 5 | ⋯ | 294.2 | ⋯ | 313.1 |
| 10 | 289.3 | 300.7 | 11.4 | 320.6 |
| 20 | 287.1 | 308.5 | 21.4 | 331.3 |
| 40 | 298.6 | 320.1 | 21.5 | 346.1 |
| 80 | 298.6 | 329.0 | 30.4 | 373.2 |



FIG. 1. Continuous heating DSC curves obtained at different heating rates. The inset shows the Kissinger plots. Arrows indicate the isothermal annealing temperatures.
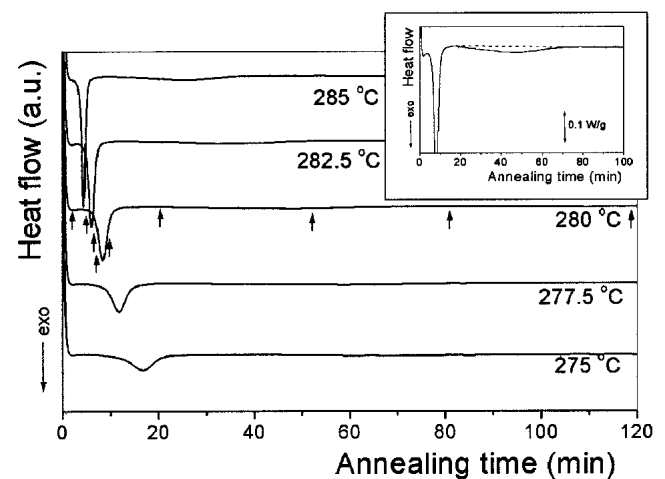


FIG. 2. Isothermal DSC-curves obtained at different annealing temperatures ($T_{ann}$). The arrows indicate the length of the pre-anneals at $T_{ann}$ = 280 °C. The inset shows the isothermal DSC curve carried out at $T_{ann}$ = 280 °C.

the isothermal anneals. The inset shows the enlargement of the isothermal curve carried out at $T_{ann}$ = 280 °C, confirming the presence of the two exothermic heat releases. The results of these anneals are summarized in Table II. As shown in Table II and presented in Fig. 3, as the annealing temperature is increased, the values of the enthalpy released during the two exothermic processes increase monotonically. This fact suggests that greater thermal stability is achieved when isothermal annealing temperature is high.

From the analysis of these curves, it could be deduced that the crystallization processes of the $Al_{85}Ni_8Ce_5Co_2$ glassy alloys occur through a nucleation and growth process.[18,19] This is contrary to what has been found for other Al-based alloys[10,12,17] in which a monotonically decreasing exothermic DSC signal was observed with no clearly defined exothermic peaks.

From the shift of the $t_{peak}$ as a function of $T_{ann}$, the apparent activation energy ($E_a^{iso}$) was determined and found to have 3.5 ± 0.5 and 2.3 ± 0.5 eV for the first and second peaks, respectively. These values are similar to those obtained during continuous heating experiments.

## B. Microstructural development

Figure 4 shows the XRD patterns of the $Al_{85}Ce_5Ni_8Co_2$ as-quenched ribbon and continuously heated up to 313 and 550 °C. The as-quenched state exhibits a broad and symmetric halo around $2\theta$ = 38, which is typical for a fully amorphous phase.

After the first crystallization stage (continuous heating at 20 K min$^{-1}$ up to 313 °C), $\alpha$–Al, orthorhombic $Al_{11}Ce_3$, orthorhombic $Al_3Ni$, and unidentified metastable phase(s) were formed, superimposed with a faint amorphous background. For the two major phases, the average crystallite size was about 31 ± 2 nm. For the studied alloy with Ce > 4 at.%, the lack of a primary crystallization of $\alpha$–Al during the first process of the devitrification is in agreement with the work on the Al–Ni–Ce system by Tsai *et al.*[12]

The final microstructure developed after the second crystallization peak (continuous heating at 20 K min$^{-1}$ up to 550 °C), consists of $\alpha$–Al, hexagonal $Al_3Ce$, orthorhombic $Al_3Ni$, and monoclinic $Al_9Co_2$ phases, as well as some unidentified ones. The Bragg peaks become

more intense and narrower, indicating grain coarsening. The mean grain size of the $\alpha$–Al and $Al_3Ce$ were found to be 48 ± 4 and 51 ± 4 nm, respectively.

The microstructure of the isothermally crystallized samples was also monitored by XRD. Figure 5 shows the XRD patterns of the $Al_{85}Ce_5Ni_8Co_2$ glassy alloy annealed for 120 min at temperatures between 275–285 °C. From the analysis of Fig. 5, the same crystalline phases were obtained as those found after a continuous heating up to 550 °C, in agreement with the DSC results. The evaluated mean grain sizes of the two major phases are listed in Table II and plotted in Fig. 6. In the figure an increase of the average grain sizes with increasing $T_{ann}$ temperature is visible; however, the mean grain sizes remain below those obtained by continuous heating up to 550 °C. Due to the relatively low peak-intensities, other grain-size values cannot be determined.

## IV. DISCUSSION

### A. Kinetics of crystallization

Theoretically, the crystallization kinetics can be studied by isothermal DSC experiments, but in fact, it rarely occurs in the literature due to a baseline instability and/or insufficient accuracy of the DSC measurements. However, as can be seen in Fig. 2, it appears that these drawbacks have been overcome in the case of the present study.

Figure 7 shows the crystalline transformed fractions of the first exothermic peak obtained directly from the isothermal curves according to the following equation:

$$x(t) = \frac{\int_0^t \dot{H}(t)dt'}{\Delta H_1^{iso}} \quad , \qquad (1)$$

where $x(t)$ is the measured transformed fraction, $\dot{H}$ the measured heat flow, and $\Delta H_1^{iso}$ the enthalpy of the first crystallization stage during the isothermal annealing. It is clear that as the annealing temperature increases, the transformation is completed in shorter times.

An alternative method for investigating the crystallization kinetics under isothermal conditions is continuous-heating DSC after partial isothermal annealings (pre-anneals). If the total enthalpy release (during the

TABLE II. Phase transformation parameters evaluated from the isothermal annealing for the $Al_{85}Ce_5Ni_8Co_2$ alloy. See text for notation.

| $T_{ann}$ (°C) | $T_0$ (sec) | $t_{peak,1}$ (sec) | $\Delta H_1^{iso}$ (J/g) | $t_{peak,2}$ (sec) | $\Delta H_2^{iso}$ (J/g) | $\Delta H_1^{iso} + \Delta H_2^{iso}$ (J/g) | $d_{Al3Ce}$ (nm) | $d_{Al}$ (nm) |
|---|---|---|---|---|---|---|---|---|
| 275 | 316 | 1005 | 55 ± 4 | 4578 | ⋯ | ⋯ | 28 ± 2 | 24 ± 2 |
| 277.5 | 287 | 707 | 60 ± 4 | 3528 | 27 ± 2 | 87 ± 6 | 28 ± 2 | 24 ± 2 |
| 280 | 243 | 503 | 63 ± 4 | 2890 | 32 ± 2 | 95 ± 7 | 31 ± 2 | 32 ± 2 |
| 282.5 | 183 | 363 | 68 ± 5 | 2084 | 33 ± 2 | 102 ± 7 | 40 ± 3 | 31 ± 2 |
| 285 | 143 | 262 | 72 ± 5 | 1552 | 33 ± 2 | 104 ± 7 | 39 ± 3 | 35 ± 2 |

2142

J. Mater. Res., Vol. 17, No. 8, Aug 2002

pre-anneal and during the nonisothermal scan) is assumed constant, the transformed crystalline fraction in the pre-anneal can be evaluated by measuring the residual area of the crystallization peak in the nonisothermal DSC curves obtained after the pre-anneals. The transformed volume fraction during the first crystallization stage can be calculated as

$$x(t) = \frac{\Delta H_1 - \Delta H_1(t)}{\Delta H_1} \quad , \qquad (2)$$

where $\Delta H_1(t)$ is the measured enthalpy release during the continuous heating after the pre-anneal for time $t$.

Figure 8 shows the DSC curves obtained during continuous heating (20 K min$^{-1}$) of the as-quenched ribbon and after pre-anneals at 280 °C, for 3, 6, 7, 8, and 9 min. With increasing pre-annealing time, the area of the first peak is diminished, while the area of the second peak remains practically unchanged. The corresponding evaluated values of $x(t)$ to different times are also plotted in Fig. 7. As can also be seen, the data points fit very well to the $x(t)$ curve obtained from isothermal DSC experiments, indicating that both procedures are valid for determining the transformed crystalline fraction.

The study of the crystallization kinetics was performed by combining both isothermal and continuous heating regimes. To analyze the data we assumed the following kinetic equation:

$$\frac{dx}{dt} = K(T) f(x) \quad , \qquad (3)$$



FIG. 3. Variation of the released enthalpies as a function of the annealing temperature ($T_{ann}$).



FIG. 5. XRD patterns corresponding to the isothermally annealed samples for $t_{ann}$ = 120 min at various annealing temperatures. The Bragg peaks are denoted as (▼) α–Al, (●) Al$_3$Ce, (□) Al$_3$Ni, and (?) unknown phase(s).
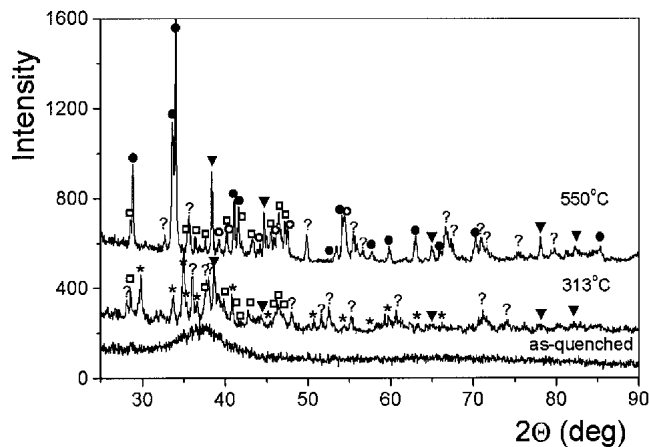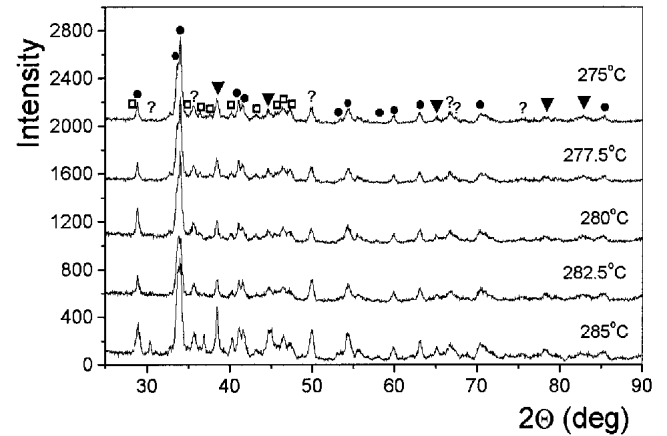


FIG. 4. X-ray patterns corresponding to the as-quenched, partially crystallized (continuous heating at 20 K min$^{-1}$ up to 313 °C), and fully crystalline (continuous heating at 20 K min$^{-1}$ up to 550 °C) states. The Bragg peaks are denoted as follows: (▼) α–Al, (●) Al$_3$Ce, (○) Al$_9$Co$_2$, (□) Al$_3$Ni, (*) Al$_{11}$Ce$_3$, and (?) unknown phase(s).
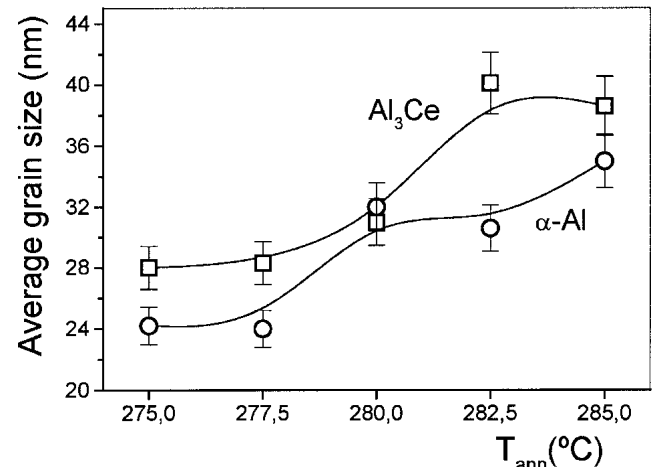


FIG. 6. Variation of the grain size of the Al$_3$Ce and α–Al as a function of the annealing temperature ($T_{ann}$).

which gives the rate of crystallization, in separate variables, as a function of the crystalline fraction $x$ and the temperature $T$. Furthermore, we assumed that the kinetic factor $K(T)$, in the limited interval explored experimentally, follows an Arrhenius behavior.

From the DSC curves, measurements of the transformed rate $dx/dt$ in both isothermal and continuous heating regimes have also been deduced.[20] To determine the best model for explaining the crystallization behavior of the $Al_{85}Ni_8Ce_5Co_2$ glassy alloy, a plot of $\ln(dx/dt) + E/RT$ against $-\ln(1 - x)$ was used, in which experimental results and theoretical predictions of several models were compared.[21] With this method, data coming from isothermal and nonisothermal treatments can be used for more complete information to the detriment of accuracy. Plots of this kind are shown in Fig. 9. The best fit to experimental values is obtained by the Johnson–Mehl–

Avrami–Erofe'ev (JMAE) model,[22] in which the transformation rate and the degree of transformation are related through the following equation:

$$\frac{dx}{dt} = n(1 - x)[-\ln(1 - x)]^{\frac{n-1}{n}} K_0 \exp\left(-\frac{E_a}{RT}\right) \quad , \qquad (4)$$

where $n$ is the Avrami exponent. For the isothermal heat treatment at $T_{ann} = 280\,°C$, a single exponent ($n = 4$) is needed to reproduce the whole crystallization in the range of $x = 0.15$ to $0.85$.

This exponent indicates 3-dimensional crystallization at constant nucleation rate.[23] A slight deviation can be observed for the linear heating data, which can arise from the limited accuracy of the activation energy. In this case more than one exponent is needed.

## B. Grain growth and interfacial energy

The evolution of the crystalline phases and their grain sizes during isothermal annealings was also monitored by x-ray diffraction. Figure 10 shows the XRD patterns obtained after annealing at $T_{ann} = 280\,°C$ for various times (indicated by arrows in Fig. 2). The first crystalline peaks appear after 6 min of annealing, coinciding with the incubation time determined from the isothermal DSC experiments. The x-ray diffractogram obtained after $t_{ann} = 20$ min exhibits similar phases to those found after linear heating at 20 K min$^{-1}$ up to 313 °C. Subsequent isothermal annealings result in the complete disappearance of $Al_{11}Ce_3$ phase and the formation of $Al_3Ce$. The final phases are identical to those obtained by continuous heating at 20 K min$^{-1}$ above the second crystallization peak (550 °C).
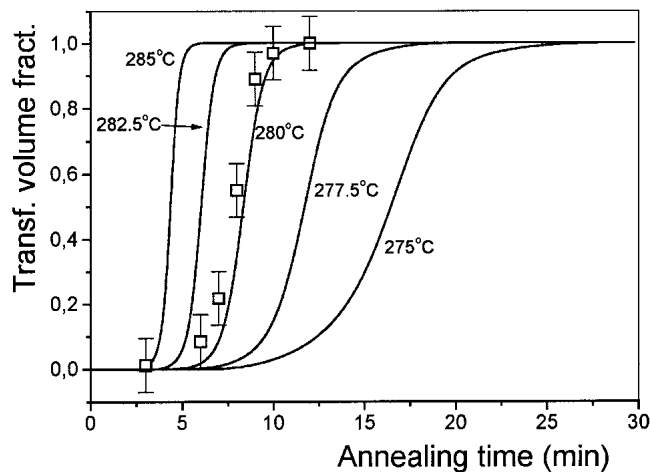


FIG. 7. Transformed volume fraction curves of the first crystallization process obtained at different annealing temperatures ($T_{ann}$). Squares represents the $x(t)$ values determined from continuous heating DSC curves following pre-anneals at $T_{ann} = 280\,°C$.
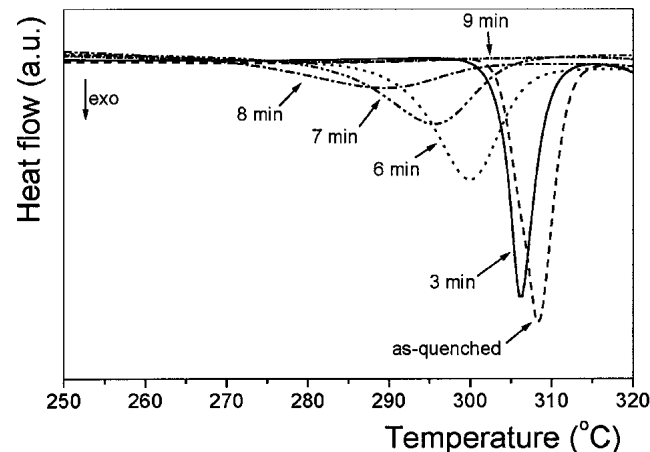


FIG. 8. Continuous heating DSC-curves obtained after pre-anneals at $T_{ann} = 280\,°C$ for different $t_{ann}$ times.
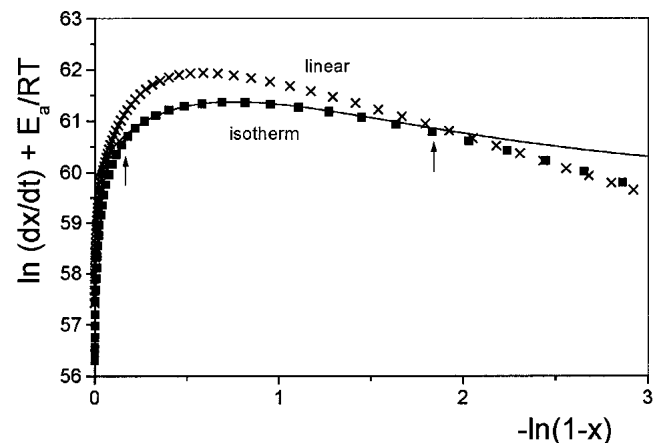


FIG. 9. Plot of $\ln(dx/dt) + E_a/RT$ versus $-\ln(1 - x)$ for two different heat treatments. The symbols (■) and (x) correspond to isothermal annealing at $T_{ann} = 280\,°C$ and to linear heating obtained at 20 K min$^{-1}$, respectively. The solid line represents the JMAE model function with an exponent of 4. The arrows corresponds to $x = 0.15$ and 0.85.

Figure 11 shows the variation of the average grain sizes of the major phases as a function of the annealing time at $T_{ann}$ = 280 °C. The mean grain size of α–Al grows throughout the overall crystallization process reaching 32 nm, according to a parabolic law, in agreement with the transmission electron microscope observations available in literature.[12,24,25].

In the case of normal isothermal grain growth, the variation of grain size can be described as

$$d^p - d_0^p = K_T t \quad , \qquad (5)$$

where $d_0$ represents the initial and $d$ the final value grain size, $K_T$ is a rate constant, and $p$ is the growth exponent. Under ideal conditions (high purity metals, high

homologous temperature) $p$ is assumed to be equal to 2; however, several factors, such as grain boundary segregation, solute drag, and second phase (Zener) drag, can often significantly alter this value. In most cases $d_0$ is often ignored, which is justified only if $d_0$ is negligible compared to $d$. Fitting Eq. (5) with $d_0$ = 0, one can obtain $p$ = 2.6 for the growth of α–Al. This exponent is somewhat higher than the ideal value and indicates that different factors can control the grain growth.[26]

During a grain-growth process from $d_1$ to $d_2$, the change of the total heat release per unit mass $\Delta H$ can be given as

$$\Delta H = \frac{6}{\rho} \bar{\gamma} \left| \frac{1}{d_1} - \frac{1}{d_2} \right| \quad , \qquad (6)$$

where $\rho$ is the sample density and $\bar{\gamma}$ is the average specific grain boundary energy. In this simple approximation it is assumed that there is no phase transformation and that the grain boundary structure and the associated specific grain boundary energy does not change significantly.

As it was shown by Révész *et al.*,[27] in different states containing the same phases, a "virtual" heat release can be introduced, which is equal to the enthalpy difference between the two states, and afterwards $\bar{\gamma}$ can be determined. According to Table II, the difference in the total enthalpy release, $\Delta H_1^{iso} + \Delta H_2^{iso}$, between annealing temperatures of 285 and 277.5 °C is 17.6 J/g. When average grain-size values of the $Al_3Ce$ and $Al$ phases at 277.5 and 285 °C were $d_1$ = 26 and $d_2$ = 37 nm, respectively, $\bar{\gamma}$ was found to be 1.2 ± 0.2 J/m². This value is on the order of the energy generally attributed to high-angle grain boundaries[28] and is similar to the value obtained by Tschöpe and Birringer on nanocrystalline platinum (1.1 J/m²) prepared by inert gas condensation method[29] and to the value obtained by Révész and Lendvai (1.3 J/m²) on ball-milled nanocrystalline iron.[30] The formation of high-angle grain boundaries indicates random crystallite orientations and independent nucleation events.



FIG. 10. XRD patterns of the isothermally annealed samples at $T_{ann}$ = 280 °C for different $t_{ann}$ times. The Bragg peaks are denoted as follows: (▼) α–Al, (●) $Al_3Ce$, (○) $Al_9Co_2$, (□) $Al_3Ni$, (*) $Al_{11}Ce_3$, and (?) unknown phase(s).



FIG. 11. Variation of the grain size of the major phases as a function of the annealing time at $T_{ann}$ = 280 °C. The dashed line corresponding to the growth of Al represents the fitted functions according to Eq. (4). The dotted lines are guides for the eye.

## V. CONCLUSIONS

The crystallization of the amorphous $Al_{85}Ce_5Ni_8Co_2$ during continuous heating and isothermal regimes takes place in two stages. In both regimes, the apparent activation energies for the two crystallization peaks determined are in good agreement. The first exothermic transformation corresponds to the crystallization of the α–Al, orthorhombic $Al_{11}Ce_3$ and $Al_3Ni$, and unidentified metastable phase(s). The final microstructure contains α–Al, $Al_3Ce$, $Al_3Ni$, and $Al_9Co_2$ phases, as well as some unidentified ones. Isothermal annealing of the as-quenched sample revealed that the first crystallization
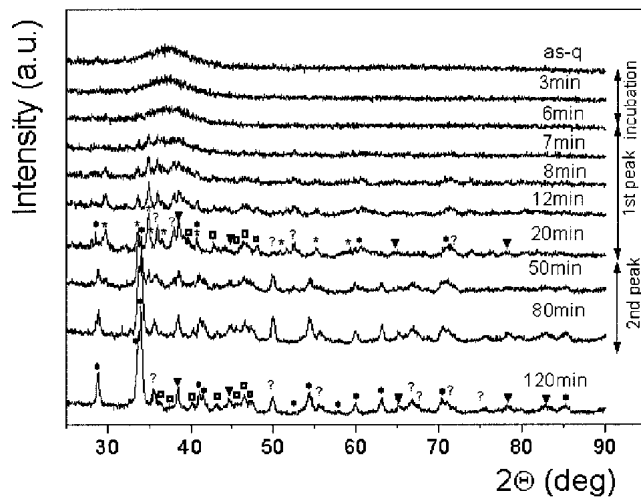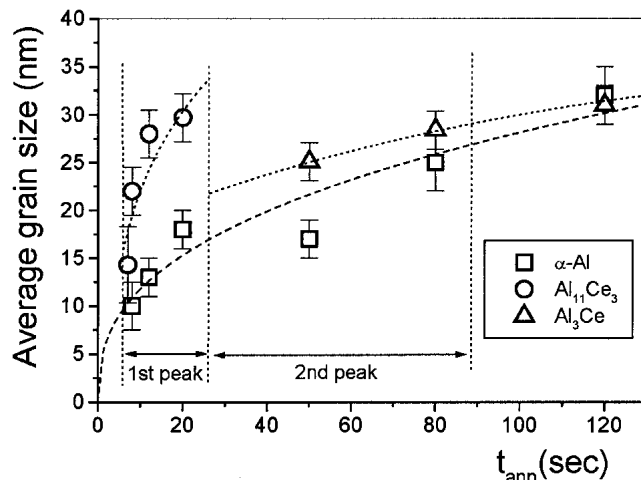
occurs through a nucleation and growth process. The crystallization mechanism of amorphous $Al_{85}Ce_5Ni_8Co_2$ during continuous heating and isothermal regimes shows JMAE kinetics with an Avrami exponent of 4, indicating 3-dimensional crystallization at constant nucleation rate. The average specific grain boundary energy corresponds to high-angle grain boundaries and indicates independent nucleation events.

## ACKNOWLEDGMENTS

## REFERENCES

1. A. Inoue, K. Ohtera, A.P. Tsai, and T. Masumoto, Jpn. J. Appl. Phys. **27,** L289 (1988).
2. Y. He, S.J. Pooh, and G.J. Shiflet, Science **241,** 1640 (1988).
3. A. Inoue, K. Ohtera, A.P. Tsai, and T. Masumoto, Jpn. J. Appl. Phys. **27,** L479 (1988).
4. W.T. Kim. M. Gogebakan, and B. Cantor, Mater. Sci. Eng. A **226–228,** 178 (1997).
5. X.Y. Jiang, Z.C. Zhong, and A.L. Greer, Philos. Mag. B **76,** 419 (1997).
6. N. Bassim, C.S. Kiminami, M.J. Kaufman, M.F. Oliveira, M.N.R.V. Perdigao, and W.J. Botta Filho, Mater. Sci. Eng. A **304–306,** 332 (2001).
7. M. Yewondwossen, R.A. Dunlap, and D.J. Lloyd, J. Phys: Condens. Matter **4,** 461 (1992).
8. A. Inoue, Y. Kawamura, H.M. Kimura, and H. Mano, Mater. Sci. Forum **360–362,** 129 (2001).
9. Á. Révész, L.K. Varga, S. Suriñach, and M.D. Baró (unpublished).
10. A. Inoue, K. Nakazato, Y. Kawamura, A.P. Tsai, and T. Masumoto, Materials. Trans. JIM **35,** 102 (1994).
11. X.Y. Jiang, Z.C. Zhong, and A.L. Greer, Mater. Sci. Eng. A **226–228,** 789 (1997).
12. A.P. Tsai, T. Kamiyama, Y. Kawamura, A. Inoue, and T. Masumoto, Acta Mater. **45,** 1477 (1997).
13. P. Schumacher and A.L. Greer, Mater. Mater. Sci. Eng. A **226–228,** 794 (1997).
14. A. Inoue, K. Ohtera, A.P. Tsai, H. Kimura, and T. Masumoto, Jpn. J. Appl. Phys. **27,** L1579 (1988).
15. H.E. Kissinger, Anal. Chem. **29,** 1702 (1957).
16. D.W. Marquardt, J. Soc. Ind. Appl. Math. **11,** 431 (1963).
17. M. Gich, T. Gloriant, S. Suriñach, A.L. Greer, and M.D. Baró, J. Non-Cryst. Solids **289,** 214 (2001).
18. L.C. Chen and F. Spaepen, Nature **336,** 366 (1988).
19. L.C. Chen and F. Spaepen, J. Appl. Phys. **69,** 679 (1991).
20. M.D. Baró. S. Suriñach, J. Malagelada, M.T. Clavaguera-Mora, S. Gialanella, and R.W. Cahn, Acta Mater. Metall. **41,** 1065 (1993).
21. S. Suriñach, M.D. Baró, M.T. Clavaguera Mora, and N. Clavaguera, J. Non-Cryst. Solids **58,** 209 (1983).
22. M. Avrami, J. Chem. Phys. **9,** 177 (1941).
23. J.W. Christian, *The Theory of Transformations in Metals and Alloys,* 2nd ed. (Pergamon, Oxford, United Kingdom, 1975).
24. Z.C. Zhong, X.Y. Jiang, and A.L. Greer, Philos. Mag. B **76,** 505 (1997).
25. T. Gloriant, D.H. Ping, K. Hono, A.L. Greer, and M.D. Baró, Mater. Sci. Eng. A **304–306,** 315 (2001).
26. H.V. Atkinson, Acta Metall. **36,** 469 (1988).
27. Á. Révész, J. Lendvai, Á. Cziráki, H.H. Liebermann, and I. Bakonyi, J. Nanosci. Nanotech. **1,** 191 (2001).
28. A.P. Sutton and K.W. Ballufi, Interfaces in Crystalline Materials (Clarendon Press, Oxford, United Kingdom, 1995).
29. A. Tschöpe and R. Birringer, Acta Metall. Mater. **41,** 2791 (1993).
30. Á. Révész and J. Lendvai, Nanostruct. Mater. **10,** 13 (1998).